LAWRENCE
LIVERMORE
NATIONAL
LABORATORY

LLNL-JRNL-718397

Examining the radiation drive asymmetries present in the High Foot series of implosion experiments at the National Ignition Facility

A. Pak, L. Divol, A. L. Kritcher, T. Ma, J. E. Ralph, L. R. Benedetti, D. T. Casey, P. M. Celliers, E. L. Dewald, T. Doeppner, J. E. Field, D. Fratanduono, L. F. Berzak Hopkins, N. Izumi, S. F. Khan, O. L. Landen, G. A. Kyrala, S. LePape, M. Millot, S. R. Nagel, H. Park, J. R. Rygg, D. K. Bradley, D. A. Callahan, D. E. Hinkel, W. W. Hsing, O. A. Hurricane, N. B. Meezan, J. D. Moody, P. Patel, H. F. Robey, M. B. Schneider, R. P. J. Town, M. J. Edwards

January 18, 2017

Physics of Plasma

Disclaimer

Examining the radiation drive asymmetries present in the High Foot series of implosion experiments at the National Ignition Facility

A. Pak,[1] L. Divol,[1] A. L. Kritcher,[1] T. Ma,[1] J. E. Ralph,[1] B. Bachmann,[1] L. R. Benedetti,[1] D. T. Casey,[1] P. M. Celliers,[1] E. L. Dewald,[1] T. Döppner,[1] J. E. Field,[1] D. E. Fratanduono,[1] L. F. Berzak Hopkins,[1] N. Izumi,[1] S. F. Khan,[1] O. L. Landen,[1] G.A. Kyrala,[2] S. LePape,[1] M. Millot,[1] J. L. Milovich,[1] A. S. Moore,[1] S. R. Nagel,[1] H-S. Park,[1] J. R. Rygg,[1] D. K. Bradley,[1] D. A. Callahan,[1] D. E. Hinkel,[1] W. W. Hsing,[1] O. A. Hurricane,[1] N. B. Meezan,[1] J. D. Moody,[1] P. Patel,[1] H. F. Robey,[1] M. B. Schneider,[1] R. P. J. Town,[1] and M.J. Edwards[1]
[1)] *Lawrence Livermore National Laboratory, Livermore, CA, 94550, USA*
[2)] *Los Alamos National Laboratory, Los Alamos, NM, 87545, USA*

(Dated: 24 February 2017)

This paper details and examines the origins of radiation drive asymmetries present during the initial High Foot implosion experiments. Such asymmetries are expected to reduce the stagnation pressure and the resulting yield of these experiments by several times. Analysis of reemission and dual axis shock timing experiments indicates that a flux asymmetry, with a P2/P0 amplitude that varies from -10 to -5 %, is present during the first shock of the implosion. This first shock asymmetry can be corrected through adjustments to the laser cone fraction. A thin shell model and more detailed radiation hydrodynamic calculations indicate that an additional negative P2/P0 asymmetry during the second or portions of the third shock is required to reach the observed amount of asymmetry in the shape of the ablator at peak implosion velocity. In conjunction with symmetry data from the x-ray self emission produced at stagnation, these models also indicate that after the initially negative P2/P0 flux asymmetry, the capsule experiences a positive P2/P0 flux asymmetry that develops at or before ∼2 ns into the peak of the laser power. Here, direct evidence for this inference, using measurements of the x-ray emission produced by the lasers irradiating the hohlraum, is presented. This data indicates that the reduction in the transmitted inner laser cone energy results from impeded propagation through the plasma associated with the ablation of the capsule target. This paper also correlates measurements of the outer cone laser deposition location with variations in the observed x-ray self emission shape from experiments conducted with nominally the same input conditions.

I. INTRODUCTION

Starting a chain of fusion reactions that produces more energy than required to initiate the process is a crucial step in the pursuit of a viable fusion energy scheme and for the study of so-called burning plasmas. Multiple inertial confinement approaches to achieving this goal are being pursued[1–4]. Common to all of these approaches is the necessity to form and confine a central volume of high pressure (>100 Gbar) deuterium-tritium (DT) plasma within a dense shell of DT fuel (>100 g/cm^3). If the pressure of the central volume can be maintained over a sufficient time duration, the surrounding fuel can be heated via alpha particle deposition initiating a cascade of fusion reactions that will release more energy, in the form of energetic neutrons, than initially supplied to the system.

In the indirectly driven inertial confinement approach being pursued at the Lawrence Livermore National Laboratory, the highest performing implosion experiments to date resulted from the so-called High Foot design that increased the level of stabilization to hydrodynamic instabilities above that of the Low Foot design that was initially pursued[5,6]. While achieving a fuel gain greater than unity[7], the yield, instead of continuing to increase, was observed to plateau as the velocity of the implosion was increased. For implosions that are symmetric or one dimensional with convergence, increasing the velocity increases the available kinetic energy of the shell. This in turn increases the amount of energy that is transferred from the shell into the internal energy of the reacting hot spot at stagnation. For an approximately constant convergence ratio, higher velocities therefore are expected to increase the hot spot pressure and yield. However, if the implosion is compressed asymmetrically there will be angular variations in the momentum in the shell that compresses and confines the central hot spot and changes in symmetry with convergence will be observed. The variations in the shell momentum desynchronize the time at which different angular elements of the shell compress the hot spot. This extends the duration of time over which kinetic shell energy is transferred into the hot spot. This lowers the amount of kinetic energy which can be transfered into internal hot spot energy at a given time and therefore reduces the stagnation pressure and performance of the implosion[8]. In the High Foot series of experiments, changes in symmetry with convergence were observed and are thought to be part of what limited the pressure and yield obtained.

Radiation drive asymmetries give rise to symmetry swings and are one effect that can limit the pressure and yield of the reacting DT plasma. Detailed radiation hydrodynamic modeling of the data was conducted with the HYDRA code[9]. This modeling used a phenomenological estimate of the radiation flux asymmetries to reproduce many of the experimental observations. Calculations performed in 3D and 2D find that with the estimated level of radiation flux asymmetries, the yield of such implosions

is reduced by ∼2-5 ×, respectively[10,11].

This work aims to understand and document the origins of the radiation drive asymmetries present during the High Foot series of experiments. A description of the asymmetry present during the first shock and how this asymmetry is thought to evolve with time will be given. Using x-ray imaging of the hohlraum emission, we will also present new evidence for a time dependent asymmetry during the peak of the x-ray drive. This late time asymmetry is consistent with the phenomenological description constructed to model the observed symmetry of the x-ray self emission at stagnation. The data suggests that the peak radiation drive asymmetry arises from a reduction in the transmission of the inner cone of the laser through the plasma associated with the target ablation. Furthermore data from x-ray imaging of the hohlraum also helps to explain variations in the shape of x-ray emission on repeated experiments conducted with the same initial conditions.

The paper is organized in the following manner. In section II, a description of the integrated implosion experiments and x-ray imaging diagnostics used will be given. Following this, section III will present the results and analysis of the measurements used to infer time dependent asymmetries. Finally in section IV, our findings will be summarized and future work will be proposed.

II. EXPERIMENT

In the indirectly driven inertial confinement approach being pursued at the Lawrence Livermore National Laboratory, a spherical capsule target comprised of an outer ablator shell with an inner shell of DT fuel is first placed at the center of a cylindrical cavity called a hohlraum. The 192 laser beams of the National Ignition Facility (NIF) are then used to irradiate the inner surface of the hohlraum, producing a radiation drive which ablates the outer surface of the capsule target. The outward ablation of material triggers the inward compression or implosion of the remaining ablator and DT fuel shell. Figure 1 a-b) details the capsule and hohlraum dimensions used in the High Foot experiments described here. In this work, gold so-called 575 hohlraums were used. Here 575 refers to the inital hohlram diameter of 5.75 mm. The hohlraums were filled with helium gas to a density of 1.6 mg/cm^3 to impede the expansion of the hohlraum wall. The capsules in this subset of the High Foot implosions are quite similar to the Rev. 5 capsule design[12]. The notable difference is that the dopant has been changed from germanium to silicon in this work[13]. Changing the dopant to silicon increased the ablation pressure and subsequent velocity of the implosion[14]. This increase in ablation pressure is due to the lower emissivity of silicon as compared to germanium at energies corresponding to the peak spectral intensity associated with the radiation drive. In addition, silicon was chosen as it provides nearly the same amount of shielding from the gold M shell radiation, but has a lower atomic number than germanium, reducing the amount of radiative losses that would occur if the doped ablator were to mix into the hot spot. These capsules have an outer radius of 1.125 mm and an outer ablator shell that consists of layers of undoped and silicon doped glow discharge polymer (GDP) material. GDP is primarily comprised of hydrocarbon (CH) with small amounts of oxygen. The 195 μm thick CH ablator shell encompasses a cryogenically cooled, solid density DT ice layer with a thickness of ∼69 μm. Figure 1 b) shows the incident pattern of laser intensity on the hohlraum wall. The intensity pattern is calculated using the VISRAD[15] program and does not account for absorpbtion, refraction or reflection from the plasma within the hohlraum. As seen in Fig. 1 b), the 192 beams of the NIF are arranged into three laser cones, two outer and one inner. Before irradiating the hohlraum the laser wavelength is frequency tripled from 1054 nm to 351 nm to reduce the growth rate of laser plasma instabilities. The temporal history of the requested combined outer cone and inner cone power for experiment N130501[16], the first High Foot layered implosion, is shown in Fig. 1 c).

The symmetry of the radiation flux that the capsule experiences can be adjusted by varying the incident inner cone fraction, defined here as, $CF_{\rm in} = P_{\rm inner}/(P_{\rm inner} + P_{\rm outer})$, where $P_{\rm inner}$ and $P_{\rm outer}$ denote the power of the inner and outer cones, respectively. The requested inner cone fraction is also shown in Fig. 1 c).

As seen in Fig. 1 c), the inner cone fraction varies in time, to account for several time dependent processes which effect symmetry. These processes include time dependent laser plasma interactions within the hohlraum, including inverse Bremsstrahlung absorption, and stimulated Raman and Brillouin scattering. These effects reduce the amount of laser power that can propagate and couple to the hohlraum cavity. Inner cone propagation is relatively more challenging as the laser beams must propagate a longer distance through the hohlraum as compared to the laser beams of the outer cone.

Indeed in this work, in order to maintain the x-ray drive from the inner cone, it was necessary to employ the cross beam energy transfer (CBET) process[17]. CBET occurs near the laser entrance hole where the inner and outer cones spatially and temporally overlap. Here energy is transferred from the outer to inner cone via an ion acoustic wave driven at the beat frequency that arises from the difference in laser frequency / wavelength of the inner and outer cones. The amount of energy transferred follows the approximate proportionality $\Delta P_{\rm inner} \propto P_{\rm inner} P_{\rm outer} n_e \Delta\lambda / T_e$. Here n_e and T_e denote the plasma density and temperature, respectively. At the NIF, the wavelength separation between the inner and outer cones can be varied, allowing for control of the amount of energy transferred. As will be discussed, in the initial High Foot experiments, it was found that the amount of power that had to be transferred from the outer to inner cone via CBET had to be increased to maintain symmetry as the magnitude and duration of the peak of the x-ray drive

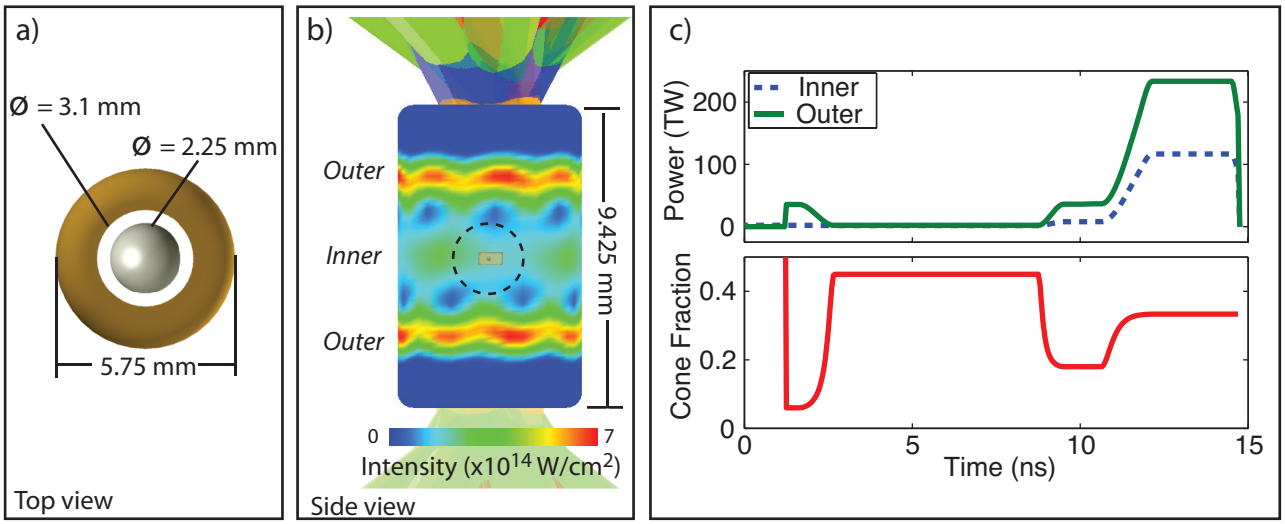

FIG. 1. (Color online) Illustration of hohlraum and capsule dimensions from above a), and from the side b). In b), the colormap represents the requested laser power deposition of the inner and two outer cones during the peak power of the laser. Also shown is the aperture through which the shape of x-ray self emission is viewed at stagnation. The dashed circle represents the original capsule diameter. c) details the requested laser power of the of the two combined outer cones (solid) and the inner cone (dashed) as well as the inner cone fraction as a function of time.

was increased. The change in the x-ray self emission symmetry as the drive duration and magnitude are increased highlights the presence of time dependent radiation drive asymmetries in these experiments.

A large effort has gone into developing methods to diagnose and then model the effects of radiation drive asymmetries throughout the implosion[18]. In the initial set of high foot experiments described here, the symmetry of the first shock was measured using the Reemission and Keyhole shock timing approaches[19,20]. Information on the integrated impact of radiation drive asymmetries during the second shock, and during the peak of the x-ray drive is inferred from radiographic measurements diagnosing the shape of the ablator shell at peak velocity and from the symmetry of the x-ray self emission at stagnation. The symmetry of the x-ray emission at stagnation is dependent on the entire temporal history of the radiation flux asymmetries and can also be modified by hydrodynamic instabilities[21] and the growth of perturbations seeded by engineering features used to support and fill the capsule[22]. Using the self emission shape to infer the symmetry of the radiation flux during the peak of the x-ray drive is therefore quite challenging[11,23].

In this work, additional data from diagnostics that image the x-ray emission from the hohlraum, is used to infer changes in the radiation symmetry during the peak of the x-ray drive. The two diagnostics used are the static x-ray imager (SXI) and the equatorial hard x-ray imager (EHXI)[24,25]. These diagnostics provide information on the location and relative magnitude of the outer and inner laser cone energy deposition. As both diagnostics are time integrated measurements, the signals are almost entirely weighted to reflect the peak of the radiation drive. The SXI and EHXI signals are recorded onto TR and MS image plate detectors,respectively. Figure 2 a)-c) illustrates the field of view of the two diagnostics.

As shown in Fig. 2 b), the EHXI diagnostic images the x-ray emission from the entire hohlraum and observes the location of the outer cones. The emission is imaged through the 30 μm thick gold hohlraum wall, the 150 μm thick aluminum thermo-mechanical package, 10 mm of plastic vacuum windows and a 30 μm thick aluminum detector filter. With this filtering and for the expected range of plasma temperatures, the detected EHXI signal is expected to be comprised primarily from photons with energies $>$ 17 keV, with the peak in the spectral response between 25-27 keV and a smaller contribution from photon energies between 10-12 keV. The position of the outer cone is found to an accuracy of $\sim \pm 50$ μm by fitting a Gaussian distribution to signal.

As seen in Fig. 2 a) and c), the lower SXI diagnostic looks through the laser entrance hole at an angle of 19° with respect to the hohlraum axis and images a portion of the hohlraum wall. Figure 2 a) shows the calculated laser intensity distribution within the hohlraum made using the VISRAD program[15]. The SXI diagnostic images an azimuthal portion of the inner and outer cones seen in Fig. 2 c). In Fig. 2 d) the synthetic SXI image has been projected into cylindrical coordinates. Here the relative intensities between the outer and inner cones for a cone fraction of 0.33 can be seen. The portion of the inner cone signal that is observed is comprised of beams that enter from the upper and lower laser entrance holes. The beams that enter at the larger 30° angle with respect to the vertical axis of the hohlraum are $\sim$1.4$\times$ more intense when projected onto the hohlraum wall compared to the 23° beams due to the steeper angle of incidence. The calculated laser intensity distribution in Fig. 2 a),

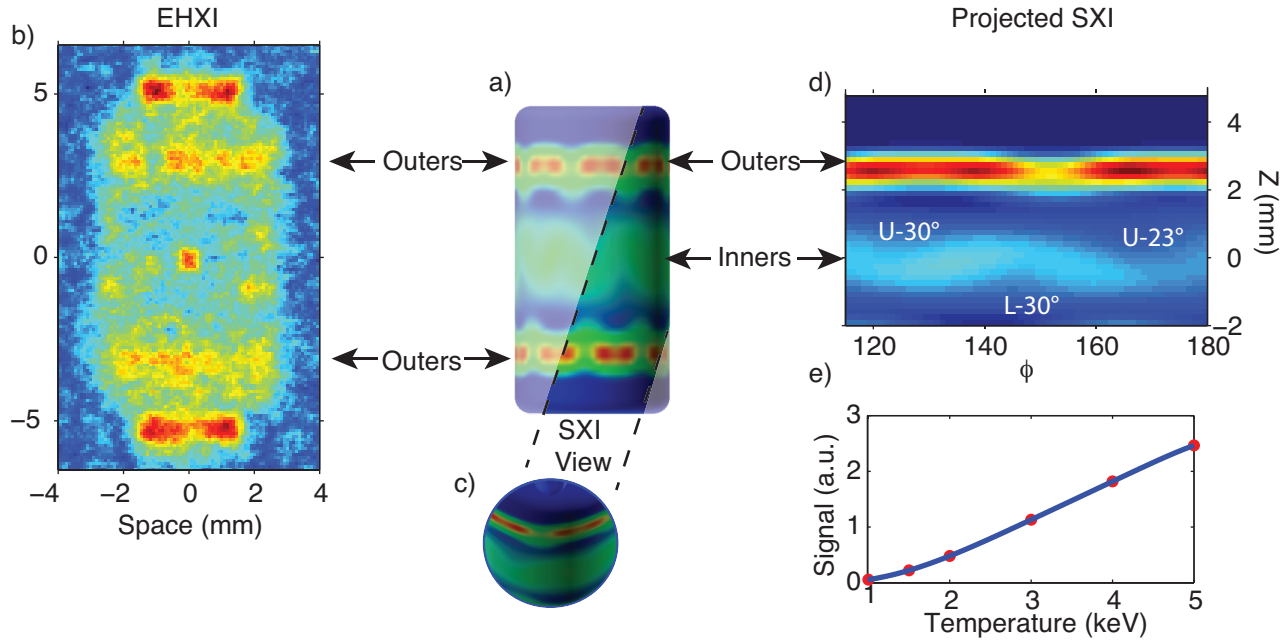

FIG. 2. (Color online) a) An illustration of the calculated laser intensity distribution inside the holhraum. Here the outer and inner cones are seen. b) An x-ray image of the hohlraum acquired using EHXI diagnostic. The outer cone location can clearly be seen, while the inner cone emission is less distinct due to the lower inner cone intensity. Also seen in the EHXI image is the central emission from the hot spot at stagnation. The bright emission above and below the outer cones is the unattenuated emission from hot plasma that is flowing out of the hohlraum. c) The SXI diagnostic line of sight and field of view. The SXI diagnostic discussed here looks up through the laser entrance hole at an angle of 19° and images emission from a portion of the inner and outer cones. d) The expected SXI signal after being projected into cylindrical coordinates. This expectation was produced using a cone fraction of 0.33. The labels on the inner cone denote whether the inner cone beams have entered through the upper (U) or lower (L) laser entrance hole and the relative angle of the inner cone propagation, either 30° or 23° with respect to the vertical hohlraum axis. e) The expected relative spectrally integrated SXI signal as a function of temperature from x-ray source produced via Bremsstrahlung. This expectation includes the 75 μm thick Kapton filtering as well as the detector response.

c) and d) were made after first decreasing the radius of the hohlraum by 500 μm to account for the amount of hohlraum wall closure. This level of hohlraum closure is inferred by measuring horizontal extent of the outer cone signal that is observed in the EHXI diagnostic. The SXI diagnostic records four time integrated images. Each image is filtered by 75 μm of Kapton. Three of the images are filtered with an additional titanium filter that is 5, 10, and 20 μm thick, respectively. This work focuses on analysis of the image filtered by only the Kapton. The peak in the spectral response of this SXI image occurs between 4-5 keV for the expected range of plasma temperatures (2-5 keV). The Kapton filtering significantly attenuates the signal from photons with energies <2 keV. An estimate of the expected SXI signal level from Bremsstrahlung emission from a plasma with an electron temperature between 1-5 keV is shown in Fig. 2 e). Here the 75 μm of Kapton filtering and image plate detector response have been included. For a fixed volume, density, and charge state, Fig. 2 e) indicates that the signal from the free-free emission scales approximately linearly with the plasma electron temperature.

Using these diagnostics to infer radiation flux asymmetries during the peak of the drive, in conjunction with reemission and dual axis shock timing experiments used to infer symmetry during the first shock, we can assess the origin of changes that were observed between the shape of the ablator at peak velocity and the shape of the x-ray self emission at stagnation. To quantify changes in symmetry, angular variations in the radiation flux symmetry, absorption of the ablator, or x-ray self emission at stagnation are fit using a Legendre polynomial basis set.

Figure 3 shows data from three companion experiments. Each experiment used a similar experimental setup with regards to the hohlraum, capsule dimensions, and laser pulse shape, power, and wavelength separation. The first of the companion experiments, N130303, was conducted using the 2D convergent ablation platform[26]. The goal of this experiment was to ascertain the shape of the ablator shell at a convergence ratio of 4-6, which occurs during the time period at which the peak implosion velocity has been reached. While this measurement is made using a hohlraum with large diagnostic windows and with a surrogate D^3He gas filled symmetry capsule, the low mode shape of the ablator at a convergence ratio of 4-6 is still thought to accurately reflect the ablator shell

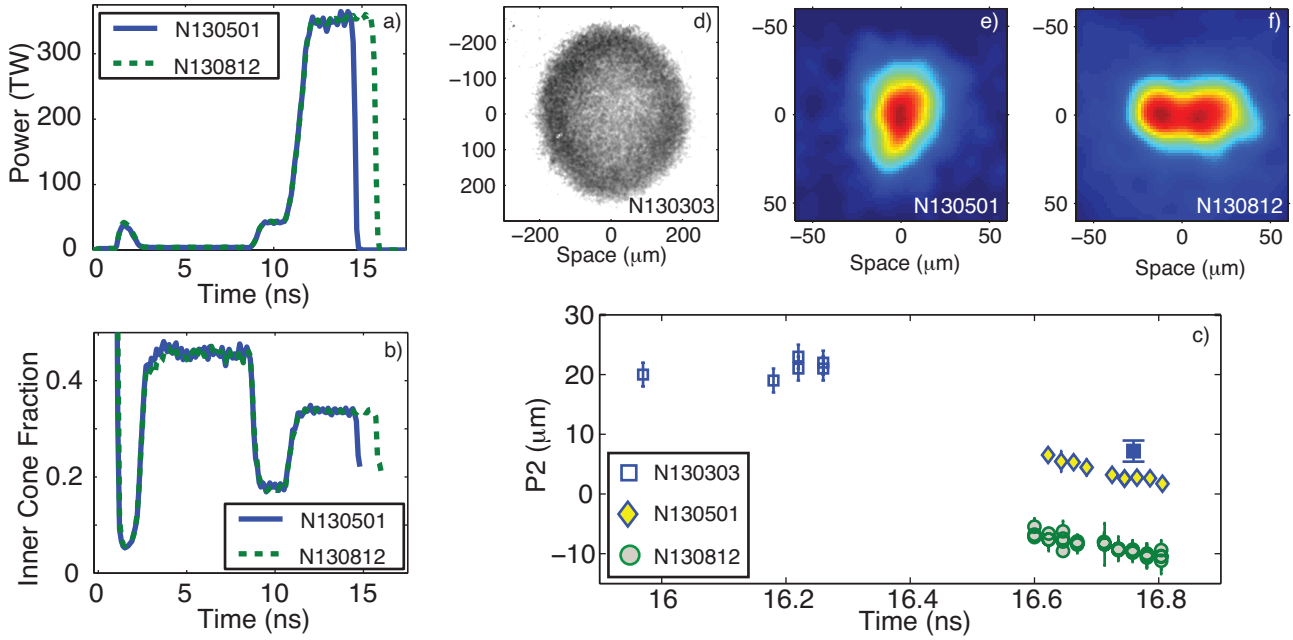

FIG. 3. (Color online) a-b) The total delivered laser power and incident cone fraction vs. time for experiment N130501 (solid line) and N130812 (dashed line). c) The amplitude of P2 as a function of time for N130501 (diamonds) and N130812 (circles). Also shown is the P2 amplitude of the in-flight ablator shell measured using radiography on experiment N130303 (open squares). The solid blue square represents the P2 amplitude of the x-ray self emission at stagnation from N130303. N130303 used the same pulse shape and cone fraction as N130501. d-f) Measurements of the in-flight shape from N130303 and x-ray self-emission at stagnation from N130501 and N130812.

shape of implosions conducted with DT fuel layers to within ∼5 μm[26]. The surrogacy in ablator shape at peak velocity between layered and symmetry tuning capsules arises from the fact that the pressure gradient across the shell and total shell mass for both targets is substantially the same. Using this surrogacy, the temporal evolution of radiation drive asymmetries can be broadly inferred from comparing the ablator shell shape, at a convergence ratio of 4-6, to the shape of x-ray self emission from higher convergence layered implosions. A radiographic image of the capsule from experiment N130303 is shown in Fig. 3 d). The ablator was observed to have a prolate shape. Over the time period of observation, as shown by the open square symbols in Fig. 3 c), Legendre mode analysis of the shape of minimum transmission indicated a P2 coefficient amplitude of 19-23± 2 μm.

The second experiment, N130501, was conducted using a capsule with a DT ice fuel layer and used the same pulse shape as N130303. The delivered laser pulse shape and cone fraction for experiment N130501 are shown in Fig. 3 a) and b), respectively. This pulse shape used a total of ∼1.3 MJ of energy, had a peak power of ∼350 TW, and a wavelength separation (before frequency tripling to 351 nm) between the outer and the inner 23° and 30° cones of 8.5 and 7.3 $\AA$, respectively. As seen in Fig. 3 e), the shape of x-ray self emission at stagnation is slightly prolate. Figure 3 c), shows that over the emission duration, the P2 magnitude of the 17% contour of peak emission, denoted by the diamond shaped symbols, decreases linearly from 6.5 to 2.7 μm. The shape of self emission at a contour level of 17% of the maximum emission value has been traditionally used to indicate the shape of the confining fuel. Comparing the shape of the ablator at peak velocity to the shape of the x-ray self emission, it is observed that the amplitude of the P2 coefficient changes by ∼16 μm. A similar change in the P2 amplitude between the self emission and ablator shape was also observed on the lower convergence 2D convergent ablation experiment N130303. This observation supports the hypothesis that, in addition to any hydrodynamic instabilities which might be present, there is also a hohlraum drive asymmetry that is modifying the shape of the assembled fuel and hot spot.

Further evidence for a time dependent asymmetry was observed on experiment N130812. This experiment also used a capsule with a DT fuel layer. As shown by the dashed line in Fig. 3 a) and b), the pulse shape and cone fraction used on N130812 are nearly identical to those used on N130501. The wavelength separation was also kept the same as N130501. The major difference in the laser pulse shape on N130812 was that the duration of the laser pulse at peak power was extended by an additional nanosecond. This extension was made to increase the implosion velocity and subsequent performance. As seen in Fig. 3 f) and by the circular symbols in Fig. 3 c), extending the laser pulse resulted in a more oblate hot

spot with a P2 coefficient amplitude of $\sim$ - 9 μm at the time of peak x-ray emission. The further decrease in the amplitude of the P2 coefficient from experiment N130501 indicates that the asymmetry amplitude is increasing in time.

Two more layered experiments N130927 and N131119 were performed with the same pulse duration as N130812. In these experiments, the peak power of the laser was increased to 395 and 410 TW, for N130927 and N131119, respectively. The power was raised to increase the implosion velocity and performance. On each of these experiments the wavelength separation was increased to maintain symmetry at stagnation. Initially, this approach worked. On N130927, the average wavelength separation was increased to 9.2/8.5 $\AA$. This seperation was 0.95 $\AA$ larger than the separation used on N130812. At these conditions the magnitude of the hot spot P2 decreased from the $\sim$ -9 μm observed on N130812, to -4 μm. As the power was further increased on N131119, the wavelength separation was also increased to the maximum available of 9.5/8.8 $\AA$. On this experiment the magnitude of the hot spot P2 increased to $\sim$ -11 μm. The inability to reduce the P2 amplitude through use of wavelength separtion indicated a lack of control over hot spot symmetry under these laser, hohlraum and capsule conditions. To reduce this amount of P2 amplitude to 0, experimentally derived scalings suggest a further increase of 1.3 $\AA$ beyond the maximum availiable wavelength separation. However, it should be noted that increasing the wavelength separation only increases the transfer if doing so brings the beat frequency of lasers closer to the resonance frequency of the plasma. As there are uncertainties on the plasma conditions at which the transfer is ocurring, the resonant frequency of the plasma is also uncertain. Therefore, the amount of transfer associated with a further increase in the wavelength separation is also uncertain. Subsequent experiments focused on using thinner capsules and uranium lined hohlraums to increase the implosion velocity while maintaining symmetry[27,28].

This set of initial High Foot experiments indicated that controlling the symmetry at stagnation as the pulse duration and peak power was increased was challenging. To understand why, this paper focuses on a subset of experiments, where measurements of radiation drive symmetry were made using surrogate tuning platforms. The measurements of the radiation flux asymmetry during the first shock will first be examined. The impact of the first shock asymmetry on the shape of the ablator at peak velocity will be estimated using a rocket model to estimate the trajectory of the ablator shell. Comparisons to calculations will also be discussed. Inferences of radiation drive asymmetries during the peak of the radiation drive will be made by examining the SXI and EHXI data.

III. RESULTS

A. First shock asymmetry

Two methods of measuring the incident radiation flux asymmetry during the first shock of the radiation drive are the reemission and dual axis shock timing techniques. The reemission experiments replace the CH capsule with a bismuth coated capsule that reemits the incident radiation drive. The reemission of the incident x-rays is viewed from the equatorial line of sight through a diagnostic window $\sim$ 2 mm in diameter. The reemission of the x-rays is temporally and spatially resolved using a gated micro-channel plate detector. The radiation flux symmetry at the capsule is quantified by decomposing the angular variation in reemission amplitude using the Legendre polynomial expansion. This method was used to assess the incident radiation flux asymmetry for the first 2.5 ns of the laser pulse.

The reemission experiment, N140227, was performed with a cone fraction 0.058. During this time period, this cone fraction was nearly the same to the cone fraction delivered on the layered experiments N130501 and N130812, which were 0.058 and 0.053, respectively. However, the reemission experiment was conducted with a wavelength separation of 6.9/6.2 $\AA$, which is on average 20% smaller than the separation used in the layered experiments. Calculations suggest that during the time period over which the reemission measurements are made, the plasma conditions support a broad range of frequiences / wavevectors over which the transfer of energy between the outer and inner laser beams can occur. These calculations indicate, that due to this broad resonance, the amount of power transfered is fairly constant for wavelength separations between 6 and 9 $\AA$[29]. Therefore, it is expected that the radiation flux asymmetry inferred from the reemission experiment will be similar to those that exist in the fully integrated layered implosion experiments, despite the difference in the wavelength separation. The diamond data point in Fig. 4 denotes the expected P2/P0 flux asymmetry at 1.5 ns for the layered experiments. The P2/P0 flux asymmetry was inferred to be -8.5 $\pm$2 % from the remission experiment N140227.

The radiation symmetry later in time is inferred using dual axis shock timing experiments. Here an inference of the radiation drive symmetry can be made through measuring the shock velocity in surrogate targets filled with cryogenic liquid deuterium[20]. As the name implies, the dual axis shock timing techniques measures the shock velocity along the polar and equatorial axes. The pressure produced by the radiation drive can be related to the shock velocity via the Hugoniot relationships and using a polytropic gas equation of state in the following manner,

$$P_f = \frac{2}{\gamma + 1} \rho_i U_s^2 \tag{1}$$

where P_f is the downstream pressure, γ is the adiabatic index, ρ_i is the upstream density and U_s is shock ve-

locity. Equation 1 is valid in the first shock of these experiments, when $2\rho_i U_s^2 \gg (\gamma-1)P_i$ where P_i is the upstream pressure of the unshocked material. Scalings to relate the pressure induced from x-ray ablation have been developed[2], and follow the approximate proportionality of $P_a = 3T_r^{3.5}$, where the units of pressure are in Mbar and the units of the radiation temperature, T_r, are in units of hundreds of eV. In the limit that the ablation pressure, P_a is approximately equal to the final downstream shock pressure, P_f, Eq. 1 can be used in conjunction with the ablation pressure proportionality to relate the ratio of the measured shock velocities at the pole and equator of the capsule to the ratio of incident temperature and therefore flux in the following manner,

$$\frac{F_{\text{pole}}}{F_{\text{equator}}} \approx \left(\frac{U_{s\ \text{pole}}}{U_{s\ \text{equator}}}\right)^{16/7} \tag{2}$$

where the radiation temperature has been related to the radiation flux, F, via $F \propto T_r^4$. To relate the ratio of flux asymmetries at the pole and equator to the normalized 2nd Legendre coefficient, the following relation was used,

$$\frac{P_2}{P_0} = \frac{\left(\frac{F_{\text{pole}}}{F_{\text{equator}}} - 1\right)}{\left(1 + \frac{1}{2}\frac{F_{\text{pole}}}{F_{\text{equator}}}\right)} \tag{3}$$

where the $P2$ amplitude has been normalized to the average flux $P0$.

The solid blue line in Fig. 4 is the inferred temporal dependence of the P2/P0 flux asymmetry as calculated using Eqn. 3. This data has been temporally smoothed over ∼250 ps. The time period over which this inference is made corresponds to the first shock of the implosion. At ∼10 ns, the second shock merges with the first shock wave and the data quality drops below that required to perform this analysis. While the reemission measurement is a temporally resolved observation of the instantaneous flux asymmetry at the capsule, the asymmetry inferred from the shock timing data is not. This is due to the finite amount of time it takes for changes in the radiation flux at the ablation front to communicate and impact the measured shock front velocity. To estimate the time at which the flux asymmetries are occurring the shock velocity data has been shifted backward in time by an estimated transit time. This transit time was calculated using the radial shock location and the tabulated values of the sound speed associated with the measured shock speed in in the plastic ablator and liquid cryogenic D2. The shaded blue region represents the uncertainty in measurement and has a half width 2.6%. This half width represents three times the standard deviation of the inferred flux over the 250 ps temporal smoothing duration. It should also be noted here that as the equatorial shock timing measurement is made at a specific azimuthal angle, it is sensitive to the laser energy in the outer and inner cones within a range of aziumthal angles ($\sim \pm 45°$)

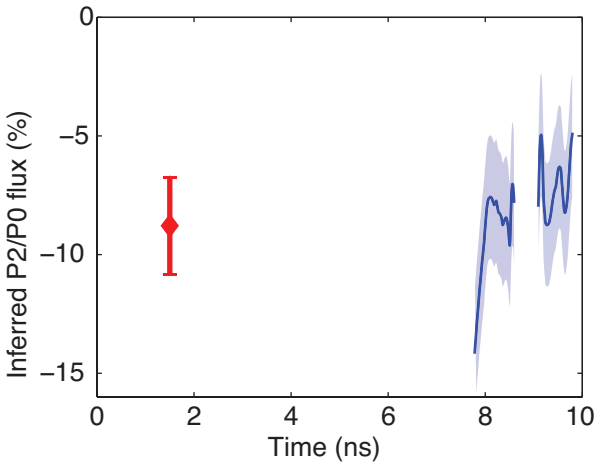

FIG. 4. (Color online) Inferred amplitude of the incident normalized P2 flux asymmetry from reemission experiment N140227, solid red diamond, and dual axis shock timing experiment N130214, solid blue line.

centered around the line of sight of detection. Differences in delivered laser energy between integrated and shock timing in this azimuth are expected to lead to variations in the P2/P0 of the incident flux by up to $\sim \pm 4\%$. The reemission and shock timing data both indicate that the first shock drive is higher around the equator than it is at the poles of the capsule, with a P2/P0 amplitude that varies from ∼-10 to -5 %.

B. Impact of first shock asymmetry at peak velocity

To estimate the impact of the observed first shock flux asymmetry on the shape of the ablator at peak velocity, a thin shell rocket model was used[30]. As previously described, this model consists of two acceleration subphases to approximate the shell trajectory. In the first phase, the trajectory is calculated by computing the down stream particle velocity for a strong shock. This is done until the shock traverses the ablator shell. After this happens, the trajectory is then calculated using the classical rocket model rate equations. In the first phase of acceleration, the velocity can be written as, $\sqrt{2P_f/((\gamma+1)\rho_i)}$. For a first shock ablation pressure of 3 Mbar, γ =2 and ρ_i=1.05 g/cm^3, an initial implosion velocity of ∼14 km/s is estimated. This model is expected to approximate the implosion trajectory up until peak velocity is reached, but is not sufficient to estimate the deceleration phase and resulting hot spot shape. In this work the thin shell rocket model was adapted to calculate the shape of the shell by computing multiple one dimensional implosion trajectories for the range of angular radiation fluxes prescribed by an applied time dependent flux asymmetry. Details of the applied flux are given in Fig. 5 a). The flux amplitude was derived from measurements of the radiation temperature on N130501. In the model, in order to

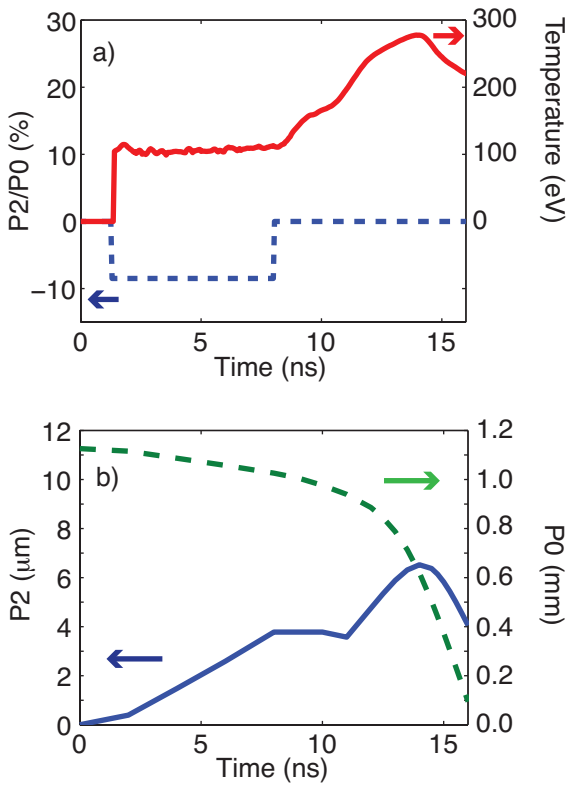

FIG. 5. (Color online) Thin shell rocket model inputs a) and the resulting calculated P2 and P0 b). a) Solid red line denotes the time history of the temperature associated with the radiation drive. Here the blue dashed line is the time dependent value of the applied normalized P2 coefficent of the radiation drive symmetry. b) The dashed green and solid blue curves represent the calculated time dependent average radius (P0), and the magnitude of P2 associated with the asymmetric shell.

reach the observed implosion velocity, the measured radiation temperature was increased by 10 eV throughout the drive. The angular flux amplitude was described using a Legendre polynomial with a prescribed time dependent normalized P2 coefficient as shown by the dashed line in Fig. 5 a). Here, to evaluate the impact of the observed first shock asymmetry, the temporal P2/P0 flux asymmetry during the first shock was fixed at -8.5% to approximate the observed asymmetries from the reemission and shock timing experiments. In the model, after the first shock, a symmetric radiation flux was applied. In this manner, the impact of the first shock asymmetry on the shape of the shell at peak velocity can be assessed and compared to the measurements described in Fig. 3 c).

By computing multiple trajectories, the temporal evolution of the ablator shell shape that results from prescribed radiation drive asymmetries can be estimated. This shell shape can be decomposed into Legendre polynomials and compared to the observed shape of the ablator shell from experiment N130303. The calculated average implosion radius, P0, in mm and the magnitude of P2 in μm are given by the dashed green and solid blue lines in Fig. 5 b), respectively. The early time flux asymmetry drives the capsule more around the equator. This causes the ablator shell radius to move further in along the equator relative to the pole and leads to an increasingly positive P2 shell coefficient, as seen in Fig. 5 b). However, during the peak of the radiation flux, the magnitude of P2 stops increasing and begins to decrease. The reversal in the slope of the P2 amplitude during the peak of the radiation flux represents the so-called phase inversion process, in which previous calculations that have applied early time asymmetries have shown, that the magnitude of the P2 in the hot spot emission at stagnation will have an opposite sign as the applied first shock flux asymmetry. This inversion results from angular differences in radius, surface area and absorbed flux for implosions which have been distorted in shape during the first shock. In the example described here in Fig. 5, the first shock flux asymmetry leads to a smaller radius around the equator than at the poles of the ablator shell at the time of peak radiation flux. This leads to a relatively higher velocity at the poles of the ablator shell as more energy is absorbed over the larger surface area at the peak of the radiation drive. The higher polar velocity causes the so-called reversal of the slope of P2 as seen in Fig. 5 b).

This thin shell rocket model indicates, that for the approximate flux asymmetry experimentally observed, the P2 amplitude associated with the ablator shell at a radius of 200 μm is 4.8 μm. Varying the P2/P0 radiation flux asymmetry by $\pm$4% in the first shock changes the P2 inferred at this radius by $\pm$2.3 μm. During the first phase of acceleration the rate of change in P2 can be estimated by $\frac{2}{3}(\frac{3}{4}U_{s\ \mathrm{pole}} - \frac{3}{4}U_{s\ \mathrm{equator}})$. The shock velocity can be written as function of incident flux asymmetry by combining Eq. 2 and Eq. 3. In this manner the rate of P2 increase with time can be written,

$$\frac{dP_2}{dt} = \frac{1}{2}U_s(1 - \left(\frac{1 - \frac{1}{2}\frac{P_2}{P_0}}{\frac{P_2}{P_0} + 1}\right)^{7/16}) \qquad (4)$$

For a first shock velocity of 21 μm/ns that is associated with a T_{rad} of 100 eV and a P_2/P_0 flux asymmetry of -8.5 %, Eq. indicates that the rate of change of P_2 with time is 0.56 μm/ns. The same rate of P2 increase with time was found during the first phase of acceleration, from 2-8 ns, using the detailed rocket model shown in Fig. 5 b).

Radiation hydrodynamic calculations were also used to assess the impact of the first shock asymmetry on the shape of the ablator at peak velocity. Applying a constant first shock flux asymmetry with a P2/P0 of -8.5% resulted in the shell having a $\sim$6.3 μm of P2 at a radius of 200 μm. Both the thin shell model and more sophisticated radiation hydrodynamic modeling therefore indicate that the observed first shock flux asymmetry does not produce the $\sim$20 μm of P2 in the ablator shell experimentally observed on N130303. Therefore, we conclude

that an additional negative P2/P0 flux asymmetry during the second and third shocks is required to distort the ablator shell to the level observed at peak velocity.

Another effect not explicitly considered in the thin shell model described above, is the radiation flux asymmetry of the hohlraum after the end of the laser pulse. After the laser pulse has turned off the radiation flux is expected to drive the capsule more at the equator and have a negative P2 asymmetry. Depending on the level, this can push the ablator shell more prolate, resulting in a larger P2 amplitude at peak velocity. However, if this was the dominant asymmetry, then one would expect to see a hot spot self emission shape with a higher P2 coefficient than observed at peak velocity. As seen in Fig. 3 c-e) a reduction in the P2 coefficient between the ablator at peak velocity and the shape of the hot spot emission is seen for the radiation drive applied on N130303 and N130501.

From this data and from inferences using the thin shell model, it appears that in addition to the observed negative P2/P0 flux asymmetry during the first shock of the implosion, in order to obtain the amplitude of P2 seen in the ablator shell at peak velocity, a negative P2/P0 flux asymmetry must also be present in the 2nd or beginning of the 3rd shock of the drive. Including the first shock asymmetry, the effect of 2nd or 3rd shock asymmetries must be sufficient to increase the P2 amplitude by $\sim$15 μm in order to reach the observed $\sim$20 μm of P2 in the ablator shell at peak velocity. To increase the P2 by this amount, the thin shell model indicates that a P2/P0 flux asymmetry of -30% or -2.5% would need to be applied in the second shock or third shock, respectively. However in order to achieve the observed change in symmetry between peak velocity and stagnation, the P2/P0 asymmetry cannot stay negative throughout the entire 3rd shock.

To model the observed change in symmetry between the shell at peak velocity and the shape of the x-ray emission at stagnation, more sophisticated two dimensional radiation hydrodynamic calculations that account for the time dependent deceleration of the ablator shell are required. In order to reproduce the implosion shape at peak velocity and at stagnation, calculations require a positive P2 (pole high) flux asymmetry to develop during the peak of the radiation drive. This is consistent with the previously discussed analysis of the thin shell model. Additionally these findings are informed from changes in the observed hot spot shape as the laser pulse was extended. As shown in Fig. 3 e-f) and previously discussed, the hot spot shape was observed to become more oblate as the pulse duration was extended between N130501 and N130812.

C. Peak flux asymmetry

The cause for this change in symmetry has been hypothesized to arise from either a reduction in the cross beam energy transfer or an increased absorption of the inner laser cone that occurs during the peak of the laser drive. Both of these hypothesis would lead to a positive, pole high radiation flux asymmetry and could account for the change in symmetry observed. To examine these hypotheses SXI data from N130501 and N130812 was compared.

Figure 6 a) and b) shows the SXI data projected into cylindrical coordinates for N130501 and N130812, respectively. Localized emission from regions irradiated by the outer and inner laser cones is observed. Due to this localization of signal, and due to the 75 μm of Kapton filtration, the observed emission is thought to be from gold hohlraum material plasma, that is close to critical density where the lasers deposit their energy. On these images, the rectangular region corresponds to the azimuth over which the profiles in Fig. 6 c) are taken. This region was chosen to compare the relative amplitude of the inner and outer cone signal. The images shown in Fig. 6 a) and b) are on the same intensity scale, while the profiles shown in Fig. 6 c) have been normalized to the peak outer cone signal amplitude on N130501. As seen from this data, as the duration of the peak power was extended, the outer cone signal on experiment N130812 increased with respect to the outer cone signal on N130501, while the inner cone signal amplitude remained similar to that observed on N130501. The time integrated SXI signal amplitude is expected to be proportional to the temperature and duration of the emission during the peak of the laser pulse. Experiments N130501 and N130812 were conducted with nearly the same power during the peak of the laser pulse. Therefore, to zero order, the increase in the signal level between N130812 and N130501 is expected to be linearly proportional to the amount of additional energy deposited as the laser pulse is extended. Averaging over all the laser beams during the peak of the laser pulse, it is found that 1.39$\times$ more energy was delivered on N130812, than on N130501. Using this approximation, an expectation of the signal level for experiment N130812 can be produced by scaling the amplitude of the SXI signal on N130501 by 1.39$\times$. The black dashed curve in Fig. 6 c) denotes this expectation. As seen in Fig. 6 c), the observed outer cone signal amplitude is within 5% of the expectation. However, the inner cone signal on N130812 was observed to increase only by $\sim$5% over N130501, well short of the $\sim$39% expected increase. This lack of inner cone signal increase clearly indicates a reduction in the transmitted inner cone power during the peak of the laser pulse. As the inner cone signal levels are nearly the same for N130501 and N130812 with $\sim$2 ns and $\sim$3 ns peak power durations, respectively, the decrease in inner cone coupling is thought to occur at or before the second nanosecond of peak power. This reduction in inner cone signal level during the peak of the laser pulse is qualitatively consistent with a pole high flux asymmetry developing during the peak of the radiation drive. Previous radiation hydrodynamic simulation modeling also required such a positive pole high flux asym-

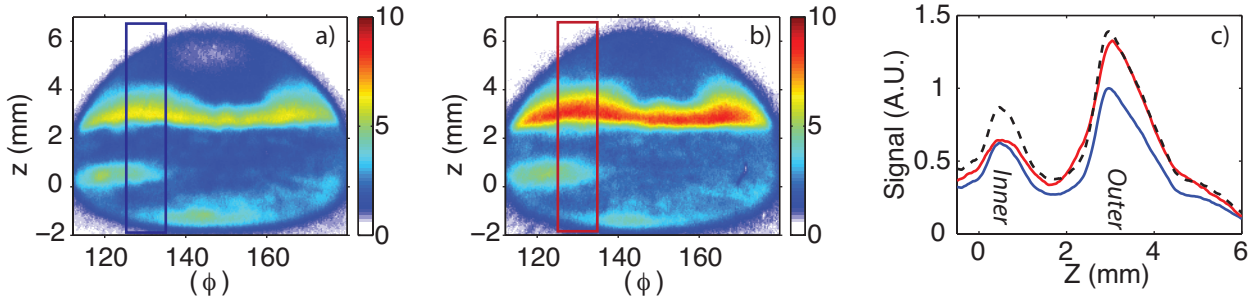

FIG. 6. (Color online) SXI data projected into cylindrical coordinates for experiment N130501 shown in a) and for experiment N130812 shown in b). Peak laser power was extended from ∼2 ns on N130501 to ∼3 ns on N130812. The blue and red rectangles represent the azimuth (125-135°) over which vertical profiles, shown in c), are taken. In c), the relative amplitude of the inner and outer beams over a 10° azimuth are shown with the solid blue and red curves representing the vertical profile from N130501 and N130812, respectively. These profiles have been normalized to the peak outer signal on N130501. The black dashed curve is the profile from N130501 multiplied by 1.39× which corresponds to the peak energy ratio between N130812 and N130501.

metry to approximately match the observed implosion shape at stagnation.

The SXI data can also be used to consider the two hypotheses for reduced inner beam propagation. The first hypothesis is that the magnitude of energy transferred from the outer to inner beams by CBET is reduced as the peak power of the laser pulse duration is extended. The second hypothesis is that the inner cone is being absorbed by either the plasma from the hohlraum wall or capsule ablator.

A time dependent reduction in CBET during the peak of the laser drive has been implemented in radiation hydrodynamic calculations to create the pole high time dependent flux asymmetry. A reduction in CBET could occur if the amplitude of the ion acoustic wave that transfers the laser energy is reduced during the peak of the laser pulse. The ion acoustic wave amplitude could decrease if there is a significant change in the ion temperature or density in the regions of the hohlraum where CBET occurs. Recent more sophositicated modeling of the plasma conditions, that temporally resolve both the stimulated Raman scattering and CBET, have indicated higher than previously predicted temperatures in the plasma where CBET occurs[31]. In the calculations this decrease occurs due to Langmuir wave induced heating of the plasma. Even with the temperature increase, the calculations indicate that a significant amount of CBET continues to occur. Understanding if there is a time dependent reduction of CBET is important because if CBET stops occurring it will strongly limit the control of symmetry during the peak of the radiation drive. If adequate control of the x-ray drive symmetry cannot be maintained, then a time dependent reduction in CBET could ultimately limit the pressures and yields obtained by this design.

Examining the SXI data from N130501 and N130812, strong evidence for a time dependent reduction in CBET is not observed. If there was a large reduction in the amount of CBET as the peak laser power was extended from ∼2 ns to ∼3 ns, then relatively more energy would go into outer cone, and relatively less energy would go into the inner cone. This scenario is not consistent with the change in the SXI inner and outer cone amplitude observed from experiment N130812, where the peak laser power was extended by 1 ns with respect to N130501. Recall, that the expectation assuming constant power levels of the inner and outer cones was previously estimated and shown by the black dashed curve in Fig. 6 c). If there is a reduction in CBET as the duration of the peak laser power is extended, then one would expect to observe an outer cone signal level that exceeds the constant power expectation. This is not observed, and as discussed the outer cone signal level is consistent with temporally constant outer cone power. Furthermore, even if there was a complete cessation of CBET, the inner cone signal level would still be expected to increase by ∼35%. This also is not observed. From these observations, it is concluded that the change in the SXI signal on experiment N130501 to experiment N130812, cannot solely be attributed to a significant reduction in the CBET. However, a reduction in CBET in addition to a time dependent increase in the outer and inner cone laser power absorption or reflection could be consistent with the observed SXI signals. To fully determine whether a strong reduction in CBET is occurring, additional experiments would be required to simultaneously temporally resolve the transmission and reflection (from stimulated Raman and Brillioun scattering) of the inner and outer cones.

The hypothesis that a time dependent pole high capsule flux asymmetry arises from losses in the inner laser cone energy from absorption or reflection by either the hohlraum or ablator plasma can also be considered by examining the SXI signal amplitudes for experiments N130501 and N130812. Comparing the observed SXI signals in Fig. 6 a) and b), to the expected pattern associated with the laser intensity in the absence of absorption shown in Fig 2 d), it is found that the observed inner cone signal azimuthal distribution shows far more vari-

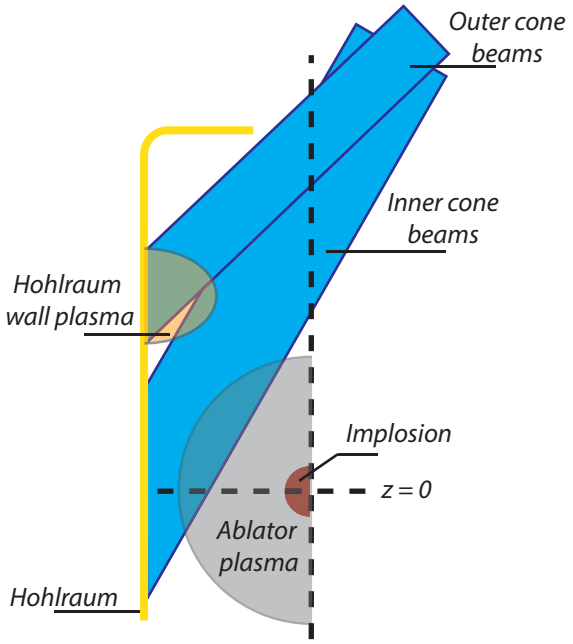

FIG. 7. (Color online) Illustration of two possible sources of inner cone absorption. Here only a portion of the hohlraum cross section, inner and outer cones are displayed for clarity. The longitudinal axis of the hohlraum and the mid plane of the hohlraum ($z = 0$) are denoted by the black dashed lines. The first source of potential absorption arises from hohlraum wall plasma ablated by the relatively higher intensity outer cone. This wall plasma can move inward and absorb energy from the inner cone. The second potential source considered is absorption of the inner cone by the plasma associated with the ablation of the capsule target. The spatial extent, density and absorption of the both the hohlraum wall and ablator plasma are dependent on the initial hohlraum gas fill density and the temporal intensity profile of the laser and x-ray drives.

ability in amplitude at a fixed z location than expected from modeling. As will be discussed, the data appears to be more consistent with the asymmetry arising from absorption or reflection of the inner laser cone energy within the ablator plasma.

The possibility that this variability in the inner cone signal level is a result of the absorption in the gold hohlraum plasma is first considered. This process is illustrated in Fig. 7. Data and calculations show that as the outer cone irradiates the hohlraum wall, the ablation of hohlraum wall material moves the radial location at which the outer laser cone deposits it's energy inward in time. If the hohlraum wall material moves radially inward far enough, the inner cone can also be absorbed at the outer cone z location before it is able to reach the mid-plane of the hohlraum. An increase of inner cone absorption at the outer cone z location would lead to a time dependent positive P2 flux asymmetry, that would drive the capsule with higher flux at the poles. If inner cone energy was being absorbed at the outer cone z location in this manner, then the expected outer cone SXI signal would be proportional to the sum of the outer cone and some fraction of the inner cone laser power. With regard to the data, it is observed that the inner cone signal level only increases by ∼5% as the laser duration at peak power is extended from ∼2 to ∼3 ns. If during experiment N130812, the remaining 95% of the inner cone energy is being absorbed by the gold hohlraum plasma at the outer cone z location, then the expected outer cone signal amplitude would be larger than the black dashed curve in Fig. 6 c) which denotes the expected signal level scaled from N130501 assuming a temporally constant rate of outer power deposition. An increase in the outer cone signal amplitude of this magnitude is not observed on experiment N130812. Additionally, if the variability in the azimuthal amplitude of the inner cone was due to the absorption of energy by the hohlraum wall plasma at the outer cone z location, a corresponding azimuthal variability in the outer cone SXI signal amplitude would be expected. However, this is not seen in the outer cone SXI signal on N130501 or N130812 in Fig. 6 a) and b). These observations do not strongly support the idea that significant amounts of the inner cone energy are being absorbed by the hohlraum wall plasma.

The inner laser cone can also be absorbed as it traverses through the lower density and lower Z plasma that has been ablated from the capsule. This scenario is illustrated in Fig. 7. As the ablator plasma expands outward it pushes against the initial helium and in flowing hohlraum wall plasma. As more time passes, and more material from the capsule is ablated, the ablator plasma density within the hohlraum increases. This leads to a time dependence on the amount of inner cone laser energy that is absorbed. As shown in Fig. 7, the ablator plasma will absorb relatively more energy from the inner cone than from the outer cone as the inner laser cone has to traverse closer to the initial capsule location, thereby experiencing higher ablator plasma densities. Additionally, the inner cone also has to traverse a longer path length in order reach the hohlraum wall.

Using this physical picture, evidence of inner cone absorption by ablator plasma can be inferred from examining the morphology of the inner cone longitudinal and azimuthal emission from the SXI data in Fig. 6 a) and b). Examining Fig. 2 d), it is observed that the inner cone SXI emission over the azimuth from ∼115-135° is produced by laser beams that enter the hohlraum from the positive z direction, or upper direction, while emission over the azimuth ∼135-165° originates from laser beams that enter the hohlraum from the negative z or lower direction. Over this range of azimuths, the upper and lower laser beams enter the hohlraum at the same angle with respect to the hohlraum axis which is approximately 30°. Examining Fig. 6 a) and b), it is observed that the signal corresponding to the upper entering and lower entering laser beams is weighted to being above and below the hohlraum mid plane in z, respectively. This distribution of the inner cone signal, which is weighted towards the direction at which the inner cone beams en-

tered the hohlraum, is indicative of absorption of the inner cone by the ablator plasma. This is because, as shown in Fig. 7 which depicts an inner cone laser beam entering from upper side of the hohrlaum, the portion of the inner laser beams that has to cross the hohlraum mid plane ($z = 0$) in order to reach the hohlraum wall, has a relatively longer path length, and therefore experiences a larger amount of absorption, than the portion of the inner laser beam that does not have to cross the mid plane. This physical picture would indicate that upper and lower entering inner laser cones will deposit relatively more energy above and below the hohlraum mid plane, respectively and this is what is observed in the SXI data. Refraction of the inner cone beams may also shift the longitudinal location of inner cone, however for these experiments it is thought that absorption is the dominant effect as the inner cone signal location and amplitude is quite similar between N130501 and N130812. To further confirm the hypothesis that absorption of the inner cone is predominately due to absorption by the ablator plasma, time resolved measurements of the extent and density of the ablator plasma can be made. Additionally detailed radiation hydrodynamic calculations could be performed to investigate what, if any, signature the absorption of the inner cone in this manner would produce on the SXI diagnostic. Absorption of the inner cone by the ablator plasma is expected to produce a significantly different SXI signal than absorption by the gold hohlraum plasma due to the lower density / charge state of the ablator plasma as well as the relatively larger spatial extent over which the inner cone laser energy is deposited.

Since the inner cone signal level did not appreciably increase as the peak laser power was extended from 2 ns on N130501 to 3 ns N130812, we conclude that the emissivity of the inner cone signal for this design reached a maximum level at a time $\leq$ 2 ns into the peak of the laser pulse. This is indicative of a reduction of inner cone propagation as the duration of peak power was extended and consistent with the development of an x-ray drive asymmetry that puts relatively more flux at the poles of the capsule during the peak of the x-ray drive. The direct inference of a peak drive asymmetry is also generally consistent with a decrease in the P2 amplitude of the x-ray self emission data as the pulse duration was extended as seen in Fig. 3 c). It is not yet clear how to quantify the degree of radiation drive asymmetry from the SXI data. One potential method is to correlate the observed inner and outer cone signal ratios either directly or through detailed calculations to an expected flux asymmetry.

D. Origins of variability in x-ray self-emission shape

The inference of radiation drive asymmetries from x-ray emission diagnostics has begun to be performed using the EHXI data to assess the impact of slight variations in the outer cone longitudinal z location on the symmetry of the implosion. The EHXI data set considered in this paper corresponds to a series of three experiments conducted with nominally the same laser, hohlraum and capsule conditions with respect to one another. In these experiments, a thinner capsule and a depleted uranium lined hohlraum was used to increase the velocity of the implosion. Details of the slightly different laser and experimental setup for this type of High Foot implosions have been reported on previously[27,28].

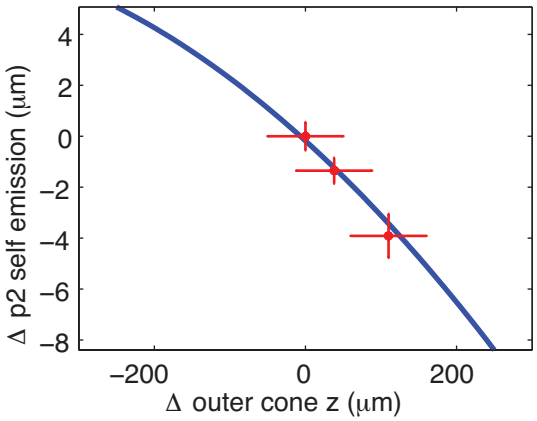

FIG. 8. (Color online) The relative change in the amplitude of the P2 in the x-ray self emission vs. the relative change in the outer cone z location. The circular red symbols correspond to the observed changes for three High Foot experiments conducted with nominally the same laser pulse shape, target and hohlraum conditions. The solid blue curve is an expectation produced using View Factor calculations and radiation hydrodynamic calculations.

Despite similar experimental inputs, the shape of the x-ray emission at stagnation varied by up to 4 μm in the amplitude of P2, which corresponds to $\sim$ 15 % P2/P0. Using the EHXI diagnostic, the average outer cone z location on these three shots was measured and found to vary by up to $\sim$110 μm. The red circles in Fig. 8 represent the relative change in the amplitude of the x-ray self emission P2 corresponding to the relative change in the outer cone z location. As the outer cone position increases and moves towards higher z locations, the radiation drive becomes relatively higher at the poles of the capsule. Recall that as the EHXI diagnostic is time integrated, the signal is strongly weighted to the peak of the laser pulse. A pole high radiation asymmetry during the peak of the radiation drive, would decrease the amplitude of the P2 coefficient at stagnation. This physical picture is consistent with observed data in Fig. 8.

An expectation of the change in the radiation drive symmetry that would result from measured changes in the outer cone z location were calculated by performing a three dimensional View Factor calculation using VISRAD[15]. In these calculations a fixed incident cone fraction of 0.2 was used. Additionally, the hohlraum radius was reduced to 2.325 mm to be consistent with the EHXI data and the capsule radius was fixed at 800 μm

to approximate the radius at the peak of the laser drive. The hohlraum albedo was set to 0.8. For these conditions, the View Factor calculations indicate a change of 1.3 % in the normalized magnitude of the P2/P0 flux asymmetry as the outer cone z location from is varied from -200 μm to +200 μm from the observed z location. To ascertain how this level of flux asymmetry changed the symmetry of the x-ray emission at stagnation, two dimensional radiation hydrodynamic calculations were used. In these calculations, a High Foot radiation drive was applied to the capsule target. The radiation drive was kept perfectly symmetric until the peak of the drive. A series of calculations were performed in which the amplitude of the P2/P0 flux asymmetry during the peak of the radiation drive was adjusted. From these calculations it was determined that the P2 magnitude of the x-ray self emission varied by $\sim$-8.5 μm / % of applied P2/P0. Multiplying this scaling to the changes in the radiation drive symmetry predicted by the View Factor calculations, an expectation for the relative change in the amplitude of P2 in the x-ray self emission for changes in the outer cone z location can be created. This relative expectation is shown by the solid curve in Fig. 8. As seen in Fig. 8, the simplified expectation reproduces the observed trend in the amplitude of P2 and indicates that changes on the order of 100 μm in the outer cone z location can appreciably change the shape of the x-ray self emission at stagnation.

The cause for the variation in the outer cone z location is still under investigation. The change in the outer cone position is not thought to arise for errors in experimental beam pointing, as it would require a systematic offset of 48 upper and lower beams. Additionally, such a systematic offset would be outside of the $\pm$50 μm accuracy of the individual beam pointing. For the separation of the outer cones to vary from shot to shot, it would require a varying systematic offset in the pointing of all the upper and lower outer cone beams. One possibility to be investigated is if differences in plasma density gradients arising from slightly different delivered laser powers or hohlraum density gas fills could lead to the differences in the outer cone refraction required to change the cone position by $\sim$100 μm.

IV. CONCLUSIONS

In this paper the radiation drive asymmetries during the first and third shocks of the initial High Foot implosion experiments have been examined. Direct experimental evidence from reemission and dual axis shock timing experiments indicates that the capsule target experienced a relatively higher x-ray flux at the waist than at the poles during the first shock of the implosion. Decomposing the radiation flux into Legendre polynomials, it was found that the normalized P2/P0 amplitude of the first shock radiation flux varied slightly from $\sim$ -10 to -5%. A thin shell rocket model and more detailed radiation hydrodynamic calculations indicate that this level of asymmetry cannot by itself cause the level of asymmetry observed in the implosion at peak velocity.

Time integrated SXI and EHXI measurements of x-ray emission produced by the lasers interacting with the hohlraum were used to infer asymmetries during the peak of the radiation drive. Examining the SXI data from experiments N130501 and N130812, the first direct evidence for a time dependent reduction of inner beam propagation was observed. The data indicates that a reduction of the inner cone energy propagation happens within 2 ns of the laser reaching peak power. This decrease of the inner laser cone propagation is expected to result in radiation flux asymmetry that is relatively higher at the poles of the capsule than at the equator. This change in radiation flux symmetry is in line with the observed decrease in the amplitude of the P2 of the x-ray self emission between experiments N130501 and N130812. Additionally, the relative amplitude and morphology of the SXI signal from these two experiments is consistent with the hypothesis that the inner cone laser energy is being absorbed by the plasma produced from the capsule ablation. Further work, such as time resolved measurements of the laser back scatter and inner beam propagation are required to verify these initial findings. Additional work is also necessary to assess whether it is possible to quantify the expected level of radiation flux asymmetry from the SXI data.

Using the measured outer cone z location from the EHXI data, coupled with View Factor and radiation hydrodynamic calculations, an expectation of the relative change in the x-ray self emission shape from the observed changes in the outer cone z location has been constructed. This simple expectation shows reasonable agreement with the change in the observed hot spot symmetry behavior. While this analysis helps to explain why differences in the shape of the x-ray self emission at stagnation were observed for experiments with nominally the same input conditions, more work is required to understand the origin of the variation in the outer cone z location.

Despite all of the measured radiation flux asymmetries and variability, the High Foot implosions are still the highest performing laser driven implosions to date. Correcting the measured asymmetries in the first shock can be done through adjustments to the laser cone fraction. Dual axis shock timing measurements and corrections to the symmetry of the second shock symmetry should also be possible. If these corrections are made, a better understanding of the magnitude of the asymmetry that develops during the third shock or peak of the radiation drive can be obtained. Strategies for mitigating this asymmetry might include, reducing the duration of the laser pulse by moving to thinner capsules, or by shortening the laser pulse by increasing the first shock strength. Both of these solutions impact other design choices such as capsule stability and fuel adiabat. One intriguing solution, which could also be used to mitigate the higher order

mode 4 radiation drive asymmetries, is to machine the initial shape and thickness of the capsule to compensate for the hohlraum drive asymmetries[32]. Using these approaches, it should be possible to recover some of the kinetic energy lost to these asymmetries and increase the stagnation pressure and performance of these implosions.

The authors sincerely thank the NIF operations staff who supported this work. This work was performed under the auspices of the U.S. Department of Energy by Lawrence Livermore National Laboratory under Contract DE-AC52-07NA27344.

[1]R. Betti and O. A. Hurrican, Nature Physics **12**, 435 (2016).
[2]J. Lindl, Physics of Plasmas (1994-present) **2**, 3933 (1995).
[3]R. S. Craxton, K. S. Anderson, T. R. Boehly, V. N. Goncharov, D. R. Harding, J. P. Knauer, R. L. McCrory, P. W. McKenty, D. D. Meyerhofer, J. F. Myatt, A. J. Schmitt, J. D. Sethian, R. W. Short, S. Skupsky, W. Theobald, W. L. Kruer, K. Tanaka, R. Betti, T. J. B. Collins, J. A. Delettrez, S. X. Hu, J. A. Marozas, A. V. Maximov, D. T. Michel, P. B. Radha, S. P. Regan, T. C. Sangster, W. Seka, A. A. Solodov, J. M. Soures, C. Stoeckl, and J. D. Zuegel, Physics of Plasmas **22**, 110501 (2015), http://dx.doi.org/10.1063/1.4934714.
[4]M. E. Cuneo, M. C. Herrmann, D. B. Sinars, S. A. Slutz, W. A. Stygar, R. A. Vesey, A. B. Sefkow, G. A. Rochau, G. A. Chandler, J. E. Bailey, J. L. Porter, R. D. McBride, D. C. Rovang, M. G. Mazarakis, E. P. Yu, D. C. Lamppa, K. J. Peterson, C. Nakhleh, S. B. Hansen, A. J. Lopez, M. E. Savage, C. A. Jennings, M. R. Martin, R. W. Lemke, B. W. Atherton, I. C. Smith, P. K. Rambo, M. Jones, M. R. Lopez, P. J. Christenson, M. A. Sweeney, B. Jones, L. A. McPherson, E. Harding, M. R. Gomez, P. F. Knapp, T. J. Awe, R. J. Leeper, C. L. Ruiz, G. W. Cooper, K. D. Hahn, J. McKenney, A. C. Owen, G. R. McKee, G. T. Leifeste, D. J. Ampleford, E. M. Waisman, A. Harvey-Thompson, R. J. Kaye, M. H. Hess, S. E. Rosenthal, and M. K. Matzen, IEEE Transactions on Plasma Science **40**, 3222 (2012).
[5]T. R. Dittrich, O. A. Hurricane, D. A. Callahan, E. L. Dewald, T. Döppner, D. E. Hinkel, L. F. Berzak Hopkins, S. Le Pape, T. Ma, J. L. Milovich, J. C. Moreno, P. K. Patel, H.-S. Park, B. A. Remington, J. D. Salmonson, and J. L. Kline, Phys. Rev. Lett. **112**, 055002 (2014).
[6]M. J. Edwards, P. K. Patel, J. D. Lindl, L. J. Atherton, S. H. Glenzer, S. W. Haan, J. D. Kilkenny, O. L. Landen, E. I. Moses, A. Nikroo, R. Petrasso, T. C. Sangster, P. T. Springer, S. Batha, R. Benedetti, L. Bernstein, R. Betti, D. L. Bleuel, T. R. Boehly, D. K. Bradley, J. A. Caggiano, D. A. Callahan, P. M. Celliers, C. J. Cerjan, K. C. Chen, D. S. Clark, G. W. Collins, E. L. Dewald, L. Divol, S. Dixit, T. Doeppner, D. H. Edgell, J. E. Fair, M. Farrell, R. J. Fortner, J. Frenje, M. G. G. Johnson, E. Giraldez, V. Y. Glebov, G. Grim, B. A. Hammel, A. V. Hamza, D. R. Harding, S. P. Hatchett, N. Hein, H. W. Herrmann, D. Hicks, D. E. Hinkel, M. Hoppe, W. W. Hsing, N. Izumi, B. Jacoby, O. S. Jones, D. Kalantar, R. Kauffman, J. L. Kline, J. P. Knauer, J. A. Koch, B. J. Kozioziemski, G. Kyrala, K. N. LaFortune, S. L. Pape, R. J. Leeper, R. Lerche, T. Ma, B. J. MacGowan, A. J. MacKinnon, A. Macphee, E. R. Mapoles, M. M. Marinak, M. Mauldin, P. W. McKenty, M. Meezan, P. A. Michel, J. Milovich, J. D. Moody, M. Moran, D. H. Munro, C. L. Olson, K. Opachich, A. E. Pak, T. Parham, H.-S. Park, J. E. Ralph, S. P. Regan, B. Remington, H. Rinderknecht, H. F. Robey, M. Rosen, S. Ross, J. D. Salmonson, J. Sater, D. H. Schneider, F. H. Sguin, S. M. Sepke, D. A. Shaughnessy, V. A. Smalyuk, B. K. Spears, C. Stoeckl, W. Stoeffl, L. Suter, C. A. Thomas, R. Tommasini, R. P. Town, S. V. Weber, P. J. Wegner, K. Widman, M. Wilke, D. C. Wilson, C. B. Yeamans, and A. Zylstra, Physics of Plasmas **20**, 070501 (2013), http://dx.doi.org/10.1063/1.4816115.
[7]O. A. Hurricane, D. A. Callahan, D. T. Casey, P. M. Celliers, C. Cerjan, E. L. Dewald, T. R. Dittrich, T. Doppner, D. E. Hinkel, L. F. Berzak-Hopkins, J. L. Kline, S. L. Pape, T. Ma, A. G. MacPhee, J. L. Milovich, A. Pak, H.-S. Park, P. K. Patel, B. A. Remington, J. D. Salmonson, P. T. Springer, and R. Tommasini, Nature **506**, 343 (2014).
[8]A. L. Kritcher, R. Town, D. Bradley, D. Clark, B. Spears, O. Jones, S. Haan, P. T. Springer, J. Lindl, R. H. H. Scott, D. Callahan, M. J. Edwards, and O. L. Landen, Physics of Plasmas **21** (2014).
[9]M. M. Marinak, G. D. Kerbel, N. A. Gentile, O. Jones, D. Munro, S. Pollaine, T. R. Dittrich, and S. W. Haan, Phys. Plasmas **8**, 2275 (2001).
[10]A. L. Kritcher, D. E. Hinkel, D. A. Callahan, O. A. Hurricane, D. Clark, D. T. Casey, E. L. Dewald, T. R. Dittrich, T. Dppner, M. A. B. Garcia, S. Haan, L. F. B. Hopkins, O. Jones, O. Landen, T. Ma, N. Meezan, J. L. Milovich, A. E. Pak, H.-S. Park, P. K. Patel, J. Ralph, H. F. Robey, J. D. Salmonson, S. Sepke, B. Spears, P. T. Springer, C. A. Thomas, R. Town, P. M. Celliers, and M. J. Edwards, Physics of Plasmas **23**, 052709 (2016).
[11]D. S. Clark, C. R. Weber, J. L. Milovich, J. D. Salmonson, A. L. Kritcher, S. W. Haan, B. A. Hammel, D. E. Hinkel, O. A. Hurricane, O. S. Jones, M. M. Marinak, P. K. Patel, H. F. Robey, S. M. Sepke, and M. J. Edwards, Physics of Plasmas **23**, 056302 (2016).
[12]S. W. Haan, J. D. Lindl, D. A. Callahan, D. S. Clark, J. D. Salmonson, B. A. Hammel, L. J. Atherton, R. C. Cook, M. J. Edwards, S. Glenzer, A. V. Hamza, S. P. Hatchett, M. C. Herrmann, D. E. Hinkel, D. D. Ho, H. Huang, O. S. Jones, J. Kline, G. Kyrala, O. L. Landen, B. J. MacGowan, M. M. Marinak, D. D. Meyerhofer, J. L. Milovich, K. A. Moreno, E. I. Moses, D. H. Munro, A. Nikroo, R. E. Olson, K. Peterson, S. M. Pollaine, J. E. Ralph, H. F. Robey, B. K. Spears, P. T. Springer, L. J. Suter, C. A. Thomas, R. P. Town, R. Vesey, S. V. Weber, H. L. Wilkens, and D. C. Wilson, Physics of Plasmas **18**, 051001 (2011).
[13]D. G. Hicks, N. B. Meezan, E. L. Dewald, A. J. Mackinnon, R. E. Olson, D. A. Callahan, T. Dppner, L. R. Benedetti, D. K. Bradley, P. M. Celliers, D. S. Clark, P. D. Nicola, S. N. Dixit, E. G. Dzenitis, J. E. Eggert, D. R. Farley, J. A. Frenje, S. M. Glenn, S. H. Glenzer, A. V. Hamza, R. F. Heeter, J. P. Holder, N. Izumi, D. H. Kalantar, S. F. Khan, J. L. Kline, J. J. Kroll, G. A. Kyrala, T. Ma, A. G. MacPhee, J. M. McNaney, J. D. Moody, M. J. Moran, B. R. Nathan, A. Nikroo, Y. P. Opachich, R. D. Petrasso, R. R. Prasad, J. E. Ralph, H. F. Robey, H. G. Rinderknecht, J. R. Rygg, J. D. Salmonson, M. B. Schneider, N. Simanovskaia, B. K. Spears, R. Tommasini, K. Widmann, A. B. Zylstra, G. W. Collins, O. L. Landen, J. D. Kilkenny, W. W. Hsing, B. J. MacGowan, L. J. Atherton, and M. J. Edwards, Physics of Plasmas **19**, 122702 (2012).
[14]D. G. Hicks, N. B. Meezan, E. L. Dewald, A. J. Mackinnon, R. E. Olson, D. A. Callahan, T. Dppner, L. R. Benedetti, D. K. Bradley, P. M. Celliers, D. S. Clark, P. D. Nicola, S. N. Dixit, E. G. Dzenitis, J. E. Eggert, D. R. Farley, J. A. Frenje, S. M. Glenn, S. H. Glenzer, A. V. Hamza, R. F. Heeter, J. P. Holder, N. Izumi, D. H. Kalantar, S. F. Khan, J. L. Kline, J. J. Kroll, G. A. Kyrala, T. Ma, A. G. MacPhee, J. M. McNaney, J. D. Moody, M. J. Moran, B. R. Nathan, A. Nikroo, Y. P. Opachich, R. D. Petrasso, R. R. Prasad, J. E. Ralph, H. F. Robey, H. G. Rinderknecht, J. R. Rygg, J. D. Salmonson, M. B. Schneider, N. Simanovskaia, B. K. Spears, R. Tommasini, K. Widmann, A. B. Zylstra, G. W. Collins, O. L. Landen, J. D. Kilkenny, W. W. Hsing, B. J. MacGowan, L. J. Atherton, and M. J. Edwards, Physics of Plasmas **19**, 122702 (2012).
[15]J. MacFarlane, JOURNAL OF QUANTITATIVE SPECTROSCOPY & RADIATIVE TRANSFER **81**, 287 (2003).
[16]Experiments are denoted by the year, month, and date of their execution. N130501 corresponds to an experiment conducted May 1 2013.
[17]P. Michel, L. Divol, E. A. Williams, S. Weber, C. A. Thomas, D. A. Callahan, S. W. Haan, J. D. Salmonson, S. Dixit, D. E. Hinkel, M. J. Edwards, B. J. MacGowan, J. D. Lindl, S. H. Glen-

zer, and L. J. Suter, Phys. Rev. Lett. **102** (2009), 10.1103/PhysRevLett.102.025004.

[18]R. P. J. Town, D. K. Bradley, A. Kritcher, O. S. Jones, J. R. Rygg, R. Tommasini, M. Barrios, L. R. Benedetti, L. F. B. Hopkins, P. M. Celliers, T. Dppner, E. L. Dewald, D. C. Eder, J. E. Field, S. M. Glenn, N. Izumi, S. W. Haan, S. F. Khan, J. L. Kline, G. A. Kyrala, T. Ma, J. L. Milovich, J. D. Moody, S. R. Nagel, A. Pak, J. L. Peterson, H. F. Robey, J. S. Ross, R. H. H. Scott, B. K. Spears, M. J. Edwards, J. D. Kilkenny, and O. L. Landen, Physics of Plasmas **21**, 056313 (2014).

[19]E. L. Dewald, J. Milovich, C. Thomas, J. Kline, C. Sorce, S. Glenn, and O. L. Landen, Physics of Plasmas **18**, 092703 (2011).

[20]J. D. Moody, H. F. Robey, P. M. Celliers, D. H. Munro, D. A. Barker, K. L. Baker, T. Dppner, N. L. Hash, L. B. Hopkins, K. LaFortune, O. L. Landen, S. LePape, B. J. MacGowan, J. E. Ralph, J. S. Ross, C. Widmayer, A. Nikroo, E. Giraldez, and T. Boehly, Physics of Plasmas **21**, 092702 (2014).

[21]V. A. Smalyuk, R. E. Tipton, J. E. Pino, D. T. Casey, G. P. Grim, B. A. Remington, D. P. Rowley, S. V. Weber, M. Barrios, L. R. Benedetti, D. L. Bleuel, D. K. Bradley, J. A. Caggiano, D. A. Callahan, C. J. Cerjan, D. S. Clark, D. H. Edgell, M. J. Edwards, J. A. Frenje, M. Gatu-Johnson, V. Y. Glebov, S. Glenn, S. W. Haan, A. Hamza, R. Hatarik, W. W. Hsing, N. Izumi, S. Khan, J. D. Kilkenny, J. Kline, J. Knauer, O. L. Landen, T. Ma, J. M. McNaney, M. Mintz, A. Moore, A. Nikroo, A. Pak, T. Parham, R. Petrasso, D. B. Sayre, M. B. Schneider, R. Tommasini, R. P. Town, K. Widmann, D. C. Wilson, and C. B. Yeamans, Phys. Rev. Lett. **112**, 025002 (2014).

[22]S. R. Nagel, S. W. Haan, J. R. Rygg, M. Barrios, L. R. Benedetti, D. K. Bradley, J. E. Field, B. A. Hammel, N. Izumi, O. S. Jones, S. F. Khan, T. Ma, A. E. Pak, R. Tommasini, and R. P. J. Town, Physics of Plasmas **22**, 022704 (2015).

[23]R. H. H. Scott, D. S. Clark, D. K. Bradley, D. A. Callahan, M. J. Edwards, S. W. Haan, O. S. Jones, B. K. Spears, M. M. Marinak, R. P. J. Town, P. A. Norreys, and L. J. Suter, Phys. Rev. Lett. **110**, 075001 (2013).

[24]M. B. Schneider, N. B. Meezan, S. S. Alvarez, J. Alameda, S. Baker, P. M. Bell, D. K. Bradley, D. A. Callahan, J. R. Celeste, E. L. Dewald, S. N. Dixit, T. Dppner, D. C. Eder, M. J. Edwards, M. Fernandez-Perea, E. Gullikson, M. J. Haugh, S. Hau-Riege, W. Hsing, N. Izumi, O. S. Jones, D. H. Kalantar, J. D. Kilkenny, J. L. Kline, G. A. Kyrala, O. L. Landen, R. A. London, B. J. MacGowan, A. J. MacKinnon, T. J. Mccarville, J. L. Milovich, P. Mirkarimi, J. D. Moody, A. S. Moore, M. D. Myers, E. A. Palma, N. Palmer, M. J. Pivovaroff, J. E. Ralph, J. Robinson, R. Soufli, L. J. Suter, A. T. Teruya, C. A. Thomas, R. P. Town, S. P. Vernon, K. Widmann, and B. K. Young, Review of Scientific Instruments **83**, 10E525 (2012).

[25]T. Doeppner, B. Bachmann, F. Albert, P. Bell, S. Burns, J. Celeste, R. Chow, L. Divol, E. Dewald, M. Hohenberger, C. Huntington, N. Izumi, G. LaCaille, O. Landen, N. Palmer, H.-S. Park, and C. Thomas, Journal of Instrumentation **11**, P06010 (2016).

[26]J. R. Rygg, O. S. Jones, J. E. Field, M. A. Barrios, L. R. Benedetti, G. W. Collins, D. C. Eder, M. J. Edwards, J. L. Kline, J. J. Kroll, O. L. Landen, T. Ma, A. Pak, J. L. Peterson, K. Raman, R. P. J. Town, and D. K. Bradley, Phys. Rev. Lett. **112**, 195001 (2014).

[27]T. Ma, O. A. Hurricane, D. A. Callahan, M. A. Barrios, D. T. Casey, E. L. Dewald, T. R. Dittrich, T. Döppner, S. W. Haan, D. E. Hinkel, L. F. Berzak Hopkins, S. Le Pape, A. G. MacPhee, A. Pak, H.-S. Park, P. K. Patel, B. A. Remington, H. F. Robey, J. D. Salmonson, P. T. Springer, R. Tommasini, L. R. Benedetti, R. Bionta, E. Bond, D. K. Bradley, J. Caggiano, P. Celliers, C. J. Cerjan, J. A. Church, S. Dixit, R. Dylla-Spears, D. Edgell, M. J. Edwards, J. Field, D. N. Fittinghoff, J. A. Frenje, M. Gatu Johnson, G. Grim, N. Guler, R. Hatarik, H. W. Herrmann, W. W. Hsing, N. Izumi, O. S. Jones, S. F. Khan, J. D. Kilkenny, J. Knauer, T. Kohut, B. Kozioziemski, A. Kritcher, G. Kyrala, O. L. Landen, B. J. MacGowan, A. J. Mackinnon, N. B. Meezan, F. E. Merrill, J. D. Moody, S. R. Nagel, A. Nikroo, T. Parham, J. E. Ralph, M. D. Rosen, J. R. Rygg, J. Sater, D. Sayre, M. B. Schneider, D. Shaughnessy, B. K. Spears, R. P. J. Town, P. L. Volegov, A. Wan, K. Widmann, C. H. Wilde, and C. Yeamans, Phys. Rev. Lett. **114**, 145004 (2015).

[28]T. Döppner, D. A. Callahan, O. A. Hurricane, D. E. Hinkel, T. Ma, H.-S. Park, L. F. Berzak Hopkins, D. T. Casey, P. Celliers, E. L. Dewald, T. R. Dittrich, S. W. Haan, A. L. Kritcher, A. MacPhee, S. Le Pape, A. Pak, P. K. Patel, P. T. Springer, J. D. Salmonson, R. Tommasini, L. R. Benedetti, E. Bond, D. K. Bradley, J. Caggiano, J. Church, S. Dixit, D. Edgell, M. J. Edwards, D. N. Fittinghoff, J. Frenje, M. Gatu Johnson, G. Grim, R. Hatarik, M. Havre, H. Herrmann, N. Izumi, S. F. Khan, J. L. Kline, J. Knauer, G. A. Kyrala, O. L. Landen, F. E. Merrill, J. Moody, A. S. Moore, A. Nikroo, J. E. Ralph, B. A. Remington, H. F. Robey, D. Sayre, M. Schneider, H. Streckert, R. Town, D. Turnbull, P. L. Volegov, A. Wan, K. Widmann, C. H. Wilde, and C. Yeamans, Phys. Rev. Lett. **115**, 055001 (2015).

[29]J. L. Milovich, E. L. Dewald, A. Pak, P. Michel, R. P. J. Town, D. K. Bradley, O. Landen, and M. J. Edwards, Physics of Plasmas **23**, 032701 (2016).

[30]Y. Saillard, Nuclear Fusion **46**, 1017 (2006).

[31]D. J. Strozzi, D. S. Bailey, P. Michel, L. Divol, S. M. Sepke, G. D. Kerbel, C. A. Thomas, J. E. Ralph, J. D. Moody, and M. B. Schneider, Accepted Physical Review Letters (2016).

[32]D. S. Clark, C. R. Weber, V. A. Smalyuk, H. F. Robey, A. L. Kritcher, J. L. Milovich, and J. D. Salmonson, Physics of Plasmas **23**, 072707 (2016).